crystals

MDPI

Review

A Review of Transmission Electron Microscopy of Quasicrystals—How Are Atoms Arranged?

Ruitao Li [1], Zhong Li [1], Zhili Dong [2,*] and Khiam Aik Khor [1,*]

[1] School of Mechanical & Aerospace Engineering, Nanyang Technological University, 50 Nanyang Avenue, Singapore 639798, Singapore; RLI3@e.ntu.edu.sg (R.L.); ZLI013@e.ntu.edu.sg (Z.L.)

[2] School of Materials Science and Engineering, Nanyang Technological University, 50 Nanyang Avenue, Singapore 639798, Singapore

* Correspondence: ZLDONG@ntu.edu.sg (Z.D.); MKAKHOR@ntu.edu.sg (K.A.K.); Tel.: +65-6790-6727 (Z.D.); +65-6592-1816 (K.A.K.)

Academic Editor: Enrique Maciá Barber
Received: 30 June 2016; Accepted: 15 August 2016; Published: 26 August 2016

Abstract: Quasicrystals (QCs) possess rotational symmetries forbidden in the conventional crystallography and lack translational symmetries. Their atoms are arranged in an ordered but non-periodic way. Transmission electron microscopy (TEM) was the right tool to discover such exotic materials and has always been a main technique in their studies since then. It provides the morphological and crystallographic information and images of real atomic arrangements of QCs. In this review, we summarized the achievements of the study of QCs using TEM, providing intriguing structural details of QCs unveiled by TEM analyses. The main findings on the symmetry, local atomic arrangement and chemical order of QCs are illustrated.

Keywords: quasicrystal; transmission electron microscopy; symmetry; atomic arrangement

1. Introduction

The revolutionary discovery of an Al–Mn compound with 5-fold symmetry by Shechtman et al. [1] in 1982 unveiled a new family of materials—quasicrystals (QCs), which exhibit the forbidden rotational symmetries in the conventional crystallography. The ordered but aperiodic atomic arrangement in QCs enables them to possess a combination of very attractive properties, such as high hardness [2], high wear resistance [3,4], low thermal conductivity [5,6], low electrical conductivity [5,7], low surface energy [8], and high infra-red absorption [9,10]. Such properties give QCs a wide variety of potential applications, including thermal barrier coatings [11–13], wear resistant coatings [12,14,15], reinforcements in composites [11,16,17], and light absorbers [11,12]. In order to better understand and tailor the unique physical properties of QCs to meet our increasing demands for new materials, it is significant to get a comprehensive understanding of their structures.

Transmission electron microscopy (TEM) was developed to overcome the resolution limit of optical microscopy shortly after the wave-like characteristics of electrons were proposed and verified in the early 20th century [18]. Since the first instrument was built in the UK in 1936 [18], TEM has revolutionized our understanding of materials: it provides the structural, phase, crystallographic and compositional information [19–21], which has already reached atomic scale nowadays [22,23]. In addition, the capabilities of the TEM can be further extended by adding certain detectors, such as an annular dark field detector and energy dispersive X-ray spectrometry (EDX) detector. Owing to its versatility and high spatial resolution, TEM has become a major analysis tool in a range of scientific fields, including materials science [24], chemistry [25,26] and biology [27].

TEM has been intensively involved in the study of QCs since Shechtman et al. [1] discovered the icosahedral Al-Mn phase through its electron diffraction pattern analysis [28]. This is due to the

significant advantages of TEM in the characterization of QCs: the bright and dark field images can provide the morphological and microstructural information of QCs [29,30]; the forbidden symmetries (5, 8, 10, 12-fold) of the electron diffraction (selected area electron diffraction (SAED) and convergent beam electron diffraction (CBED)) patterns are the proof of the presence of QCs [31,32]; high-resolution TEM (HRTEM) allows for phase-contrast imaging of the atoms in QCs [33,34]; scanning transmission electron microscopy (STEM) combined with a high angle annular dark field (HAADF) detector provides the intuitive atomic positions in QCs [35,36]. For the critical question in the study of quasicrystalline structure—how atoms are arranged—electron diffraction patterns, HRTEM and STEM HAADF can provide distinct answers.

As TEM is an excellent method for the study of QCs, it is imperative to have a review on the progress of exploring the structure of QCs by this method. In this paper, we reviewed the research work on the diffraction patterns as well as HRTEM and STEM-HAADF analysis of QCs to get a better understanding of their quasicrystalline structure unveiled using TEM. QCs are classified into three dimensional (3D), two dimensional (2D) and one dimensional (1D) ones based on their dimensionality of quasiperiodicity: 3D QCs are quasiperiodic in all three dimensions; 2D QCs are quasiperiodic in two dimensions and periodic in the third; 1D QCs are periodic in only one dimension and periodic in the other two dimensions. Icosahedral phase is the only 3D QC found, and octagonal, decagonal and dodecagonal phases are the three types of 2D QCs discovered to date. Icosahedral and decagonal QCs constitute a vast majority of the QCs known thus far, and have been extensively studied; other QCs only exist in a few alloys, and have been much less investigated. Therefore, our review is focused on the study of icosahedral and decagonal QCs using TEM, with other QCs briefly discussed. Owing to the absence of a unit cell and the inflation–deflation property of the tiling structure, it is difficult to solve a 3D quasicrystalline structure with HRTEM or HAADF-STEM. However, it is much easier to address 2D quasicrystalline structures using these two methods, because 2D QCs are the periodic stack of quasiperiodic planes. Thus, our review mainly incorporates the HRTEM and HAADF-STEM study of decagonal QCs.

2. Diffraction Pattern Analysis of QCs

When electrons pass through a thin sample, their interaction with the atoms in the sample causes a phase shift in the electron wave. Electron diffraction occurs as a result of the interference of the electron wave at the lattice planes of materials. Diffraction patterns thus reflect the atomic arrangement in the sample. For SAED, the paralleled electron beams illuminate the sample with the diffraction spots formed in the back focal plane of the objective lens, whereas convergent illumination is used to obtain diffraction discs. Typically, an area of ~0.1 μm in the sample can be selected by using a diaphragm in SAED, while the focused beam in CBED allows one to analyze an area <5 nm. Therefore, SAED is generally employed for phase and texture analysis–through the observation of symmetry and determination of reciprocal space structure by tilting in the goniometer–on a sub-micrometer to micrometer length scale, while CBED is very powerful in the determination of space group and lattice parameters on the nanometer scale.

The capability of TEM to analyze a tiny region played a very important role in the discovery of QCs. Due to the small size (around several microns) of the first quasicrystalline phase discovered in the Al–Mn alloy, diffraction patterns of TEM was the only feasible method to determine its icosahedral symmetry. For the same reason, other QCs, including octagonal and dodecagonal ones, were all first identified using TEM. Although QCs with much larger grains can now be obtained—even single crystal QCs in centimeters have been successfully prepared, diffraction pattern analysis is still extremely useful, because it can provide the information of point group, space group, thickness, strain, and lattice parameters. Both SAED and CBED are employed in the study of QCs. The former is easier to perform, while the latter can provide more information, including space group, point group, specimen thickness, and more precise lattice parameters.

2.1. SAED

2.1.1. 3D QCs

In Shechtman et al.'s [1] TEM study of Al–Mn alloy prepared by rapid cooling, three types of SAED patterns with 5-fold, 3-fold and 2-fold symmetries were obtained by tilting the specimen goniometer (Figure 1a–c). The three types of symmetries and the angles between these SAED patterns match those of icosahedral symmetries (Figure 1d,e). These SAED patterns, therefore, correspond to icosahedral symmetries; an aperiodic but ordered phase, QC, was discovered. The numbers of the three types of symmetry axes (Figure 1d) are 6, 10 and 15, respectively. Aperiodic distribution of diffraction spots in the 5-fold pattern reflects the ordered but aperiodic atomic arrangement in the icosahedral QCs. For the conventional crystals where atoms are periodically arranged, the spots in the SAED patterns are periodic, while for the amorphous materials where atoms are disordered, no discrete spots but halo rings are present in the SAED patterns.

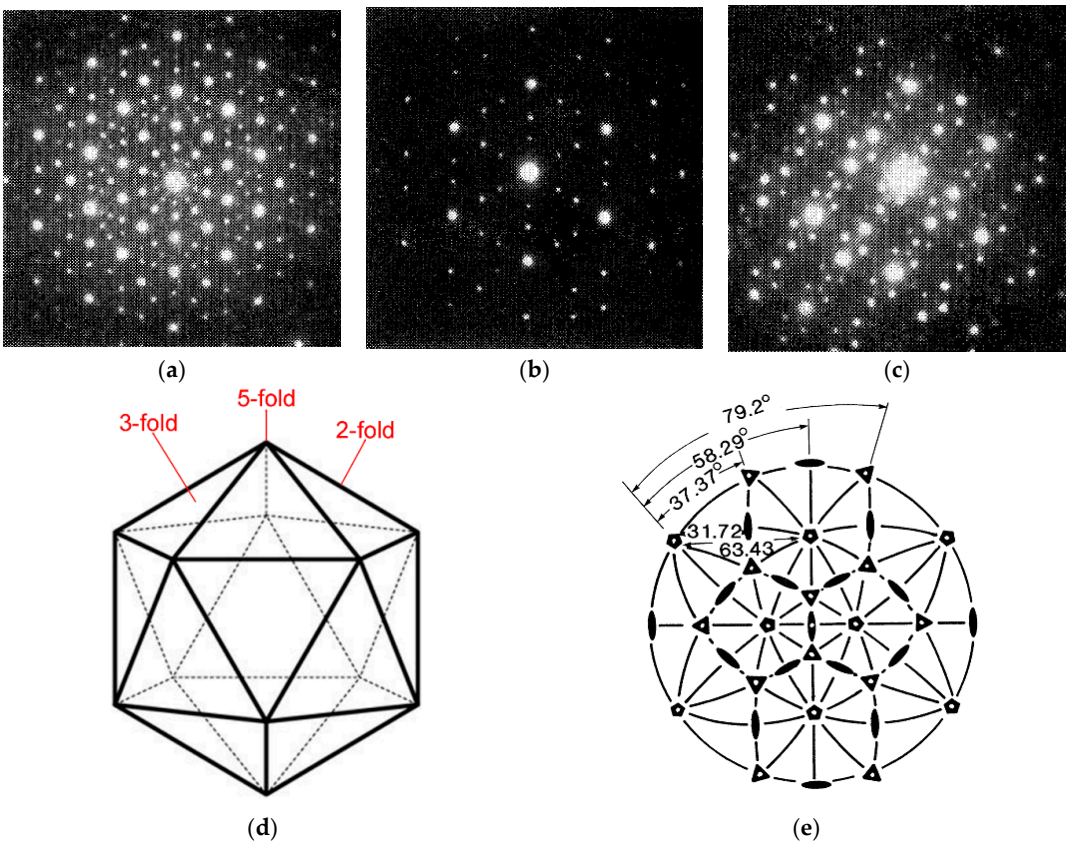

Figure 1. Icosahedral structure: SAED patterns taken along (**a**) 5-fold symmetry axis; (**b**) 3-fold symmetry axis and (**c**) 2-fold symmetry axis; (**d**) three types of symmetry axes in the icosahedral structure; (**e**) stereographic projection of the symmetry elements of the icosahedral group ((**a**–**e**) reproduced from reference [1] with permission).

The lattice of icosahedral QCs can be obtained by the projection of a 6D hypercubic into the 3D space. Theoretically, there are three types of 6D hypercubic lattice—primitive, body-centered and face-centered—corresponding to icosahedral lattice in the 3D space [37]. The lattices generated by the projection of the three different 6D hypercubic lattices into the 3D space are called primitive, body-centered and face-centered icosahedral QCs, respectively. All the icosahedral QCs discovered so far are primitive or face-centered. They can be easily distinguished by their 2-fold patterns: along their fivefold direction, the distance between the diffraction spots is inflated by τ^3 and τ ($\tau = (1 + 5^{1/2})/2$)

for primitive and face-centered icosahedral QCs, respectively [38]. The first QC discovered is primitive icosahedral phase [1]. Later, this type of icosahedral phase was found in Ag–In–Yb [39], Cd–Mg–Rare Earth [40]. The face-centered icosahedral QCs were first discovered by Tsai et al. [41] in Al–Cu–Fe and later in Al–Pd–Mn [42] and Al–Pd–Re [42], and Zn–Mg–Rare Earth [43] etc.

2.1.2. 2D QCs

Most of the 2D QCs found so far are decagonal phases, which have one 10-fold axis and two types of characteristic 2-fold axes (each type having 10 rotational axes, schematically shown in Figure 2a). The twofold axes are perpendicular to the 10-fold axis and the angle between the neighboring 2-fold axes is 18°. Along the tenfold axis, quasiperiodic atomic layers are stacked periodically. The diffraction spots are thus arranged periodically in this direction and quasiperiodically perpendicular to this direction. The periodicity along the 10-fold axis can be determined from the 2-fold symmetry patterns. Different periodicities along the 10-fold axis have been reported in different alloys: 0.4 nm [44–46], 0.8 nm [47,48], 1.2 nm [32,49] and 1.6 nm [50,51], which correspond to a stacking of 2, 4, 6 and 8 atomic layers, respectively [52,53]. Figure 2b–d are the SAED patterns taken along the periodic axis c* and two types of 2-fold symmetry axes (A and B) of decagonal $Al_{70}Ni_{20}Rh_{10}$ [31], respectively. The periodicity along c* is determined to be 0.4 nm from Figure 2c.

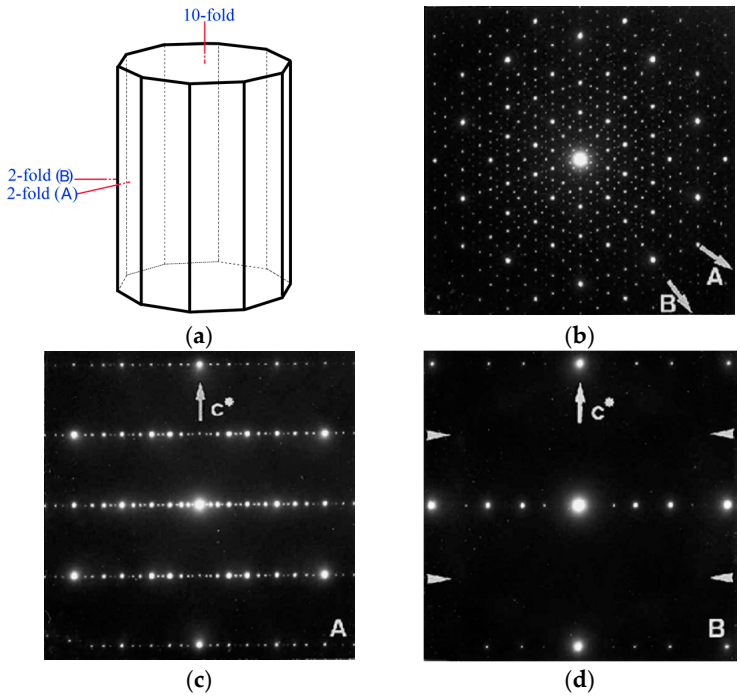

Figure 2. Decagonal structure: (**a**) schematic of decagonal structure; SAED patterns taken along (**b**) 10-fold symmetry axis, (**c**) 2-fold symmetry axis A and (**d**) 2-fold symmetry axis B of $Al_{70}Ni_{20}Rh_{10}$ (reproduced from reference [31] with permission).

From systematic absences, one can determine the lattice type as well as screw axes and glide planes, as lattice centering and symmetry elements with translation (glide planes and screw axes) cause certain reflections to have zero intensity in the diffraction pattern. In the SAED patterns taken along the 2-fold axes of decagonal phases, the absence of the reflection arrays indicates the existence of a 10_5 screw axis and/or a glide plane (Figure 2d). Such screw axis and/or glide plane have been found in Al–Ni–Rh [31], Al–Co–Ni [54], Al–Rh–Cu [55] and Al–Ni [56].

SAED patterns also reveal the structural variations of QCs with different composition or processing routes. Beeli [57] reported six decagonal variants in the Al–Co–Ni alloys: Ni-rich basic

structure, type-I superstructure, type-II superstructure, transition state between types I and II, S1 superstructure and type I superstructure of five-fold QC (Figure 3). They were obtained by altering the composition and annealing parameters. Their differences are revealed in the SAED patterns along the 10-fold axis. The basic structure has the highest structural order with sharp spots in the diffraction pattern (Figure 3a); in the diffraction pattern of the S1 structure, S1 reflections are present but S2 reflections disappear or become very weak (S1 and S2 are two types of satellite reflections denoted after Edagawa et al. [58], Figure 3b); in the SAED pattern of the type-I superstructure, both S1 and S2 reflections are present (Figure 3c); in the diffraction pattern of type-II superstructure, there are diffuse satellite reflections positioned in halfway between two strong peaks (Figure 3d), and a transition state exists between type-I and type-II (Figure 3e). In addition, a variant with 5-fold symmetry is also present: its SAED pattern (Figure 3f) shows that two spots at an angle of 36° indicated by the two arrows have different intensity; S1 and S2 reflections occur. Moreover, SAED pattern analysis indicates that in Al–Co–Ni alloys the S1 superstructure transforms into the Type-I superstructure and the Ni-rich basic structure into the S1 superstructure when annealed at 650 °C [59].

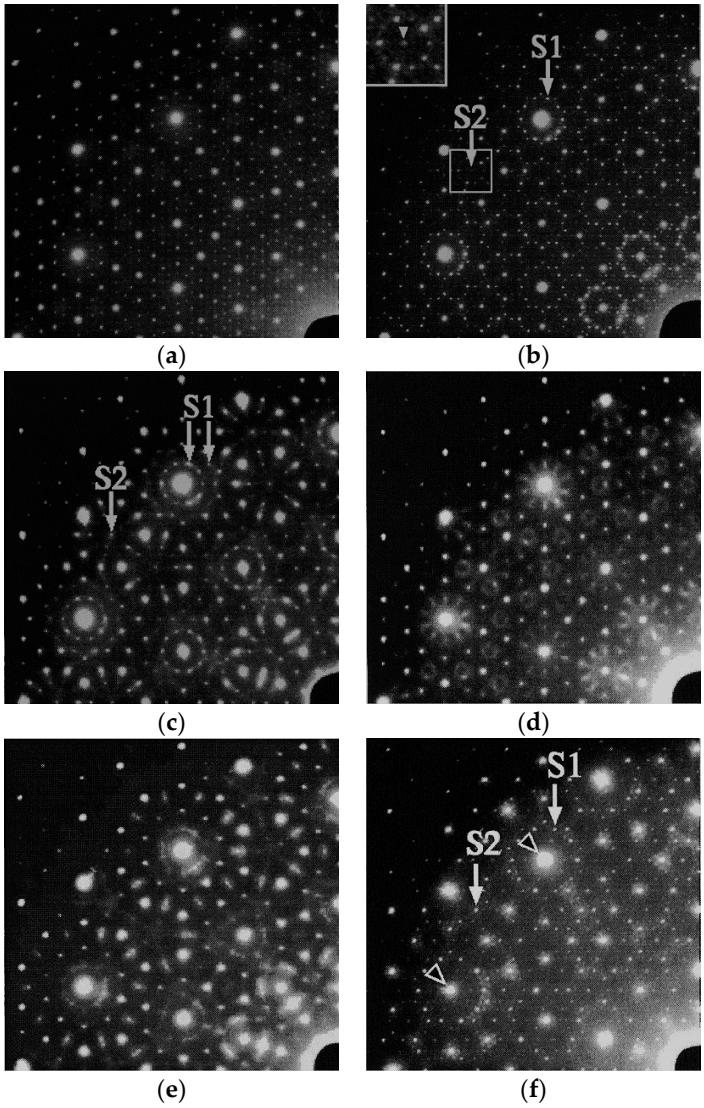

Figure 3. A quarter of SAED pattern of different decagonal Al–Co–Ni structures: (**a**) Ni-rich basic structure; (**b**) S1-type; (**c**) Type-I; (**d**) Type-II; (**e**) transition state between types I and II; and (**f**) type I superstructure of five-fold QC (reproduced from reference [57] with permission).

The diffraction patterns also reflect the order of atomic arrangement in the QCs. Diffraction streaks have been found in the SAED patterns of the decagonal structures in Al–Rh–Cu [55], Al–Co–Cu–Ni [60] and Al–Ni–Fe [61]. Saito et al. [61] proposed that these diffusion streaks may be attributed to the structural modulation. In addition, the SAED patterns also reflect the order of the decagonal structure. In the SAED patterns, the little deviation of reflections from the regular positions and the regular shapes of the reflection spots as well as the appearance of many sharp weak spots at the decagonal positions indicate that the decagonal structure is highly-ordered [62].

The first octagonal QCs were discovered in rapidly solidified V–Ni–Si and Cr–Ni–Si alloys in 1987 through SAED patterns analysis [63]. Later, such QCs were also found in Mn–Si [64], Mn–Si–Al [65] and Mo–Si–Ni [66]. These QCs have an 8-fold symmetry along the periodic axis. There are two types of 2-fold axes perpendicular to the 8-fold axis (each type having 8 rotational axes). The one-dimensional periodicity along the 8-fold axis can be determined from the SAED pattern taken along the 2-fold axis and the angle between the neighboring 2-fold axes is 22.5°. In the SAED pattern taken along the 8-fold axis, there are two types of diffraction spot rows and the space between neighboring spots in them is inflated by either $\sqrt{2}$ or $1 + \sqrt{2}$ [63].

The first dodecagonal QC was discovered in 1985 in Ni–Cr alloy. Later, such 2D QCs were also found in V–Ni(–Si) [67] and Ta-Te [68]. They have one 12-fold axis and two types of characteristic 2-fold axes (each type having 12 rotational axes). The angle between the neighboring 2-fold axes is 15°. In the SAED pattern taken along the 12-fold axis, diffraction spots are arranged on concentric dodecagons. Like decagonal and octagonal QCs, their periodicity can be determined from the 2-fold symmetry patterns.

2.2. CBED

In SAED patterns, each spot has a corresponding symmetrical spot with the same intensity, i.e., every SAED pattern is centrosymmetric. Therefore, it is difficult to definitely determine the symmetries of the materials merely based on SAED patterns. By contrast, in CBED patterns, dynamical contrast within the disks provides adequate information for one to determine the point group unambiguously.

2.2.1. Icosahedral QCs

Theoretically, there exist two icosahedral point groups: 235 and $m\bar{3}\bar{5}$ [69]. The former is noncentrosymmetric with no mirror symmetry while the latter is centrosymmetric. They can be differentiated by CBED analysis, which requires high quality QC samples with few strains. The stable icosahedral QCs have fewer strains than the metastable ones, so they can provide better diffraction patterns [70]. The CBED analysis on stable icosahedral Al–Cu–Fe reveals that it has a point group of $m\bar{3}\bar{5}$ [70,71]. Such analysis on Al–Mn–Si [72], Al–Cu–Li [73] and Al–Si–Cu [74] icosahedral QCs, also indicates that these icosahedral QCs have a point group of $m\bar{3}\bar{5}$. Actually, all the icosahedral QCs known to date are centrosymmetric and no icosahedral QCs with point group 235 have been found.

2.2.2. Decagonal QCs

Two space groups, non-centrosymmetric $P\bar{1}0m2$ and centrosymmetric $P10_5/mmc$, have been proposed for decagonal QCs [28,46]. Like the two proposed space groups of icosahedral QCs, the two space groups of decagonal QCs can be differentiated by CBED method owing to a dynamical diffraction effect of electrons. Decagonal QCs of $Al_{64}Cu_{22}Co_{14}$ [46], $Al_{70}Ni_{15}Fe_{15}$ [61] and $Al_{70}Cu_4Co_{26}$ [75] have a space group of $P\bar{1}0m2$, while decagonal QCs of $Al_{73}Ni_{22}Fe_5$ [76], $Al_{70}Ni_{20}Rh_{10}$ [31], $Al_{70}Ni_{30-x}Co_x$ (x = 15 or 20) [77] and $Al_{70}Ni_xIr_{30-x}$ (x = 15, 17 and 20) [31] belong to $P10_5/mmc$. The CBED patterns taken along the periodic axis of $Al_{70}Cu_4Co_{26}$ [75] and $Al_{70}Ni_{20}Rh_{10}$ [31] are shown in Figure 4a,b, respectively. The former exhibits 5-fold rotational symmetry, while the latter shows 10-fold rotational symmetry.

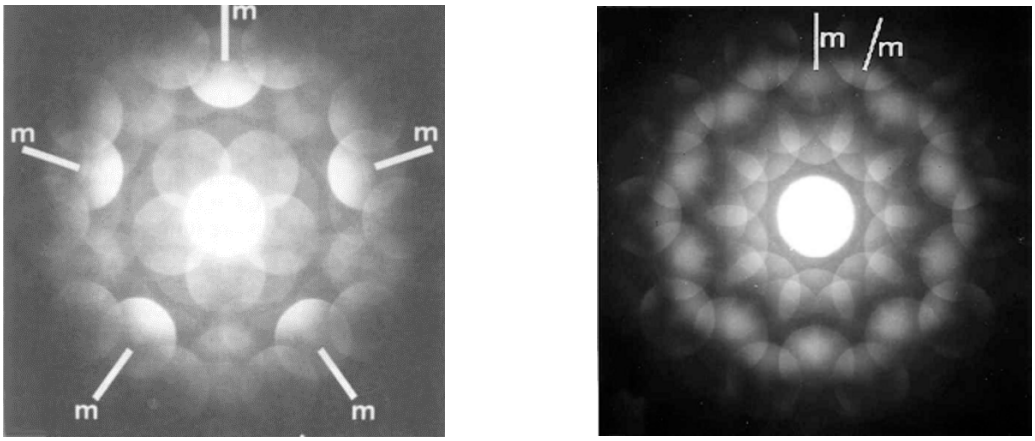

(**a**) (**b**)

Figure 4. CBED patterns taken along the periodic axis of decagonal QCs: (**a**) $Al_{70}Cu_4Co_{26}$ ($P\overline{1}0m2$) and (**b**) $Al_{70}Ni_{20}Rh_{10}$ ($P10_5/mmc$) (reproduced from reference [75] and reference [31], respectively, with permission).

It is worth mentioning that for some decagonal QCs, the space group varies due to compositional change or heat treatment. Tanaka et al. [78] prepared Al–Ni–Fe decagonal QCs with different composition by the melt-quenching method and determined their space group using CBED. Their experimental results indicate that the decagonal $Al_{70}Ni_{l0+x}Fe_{20-x}$ alloys with x in the range of 0 to 7 belong to the non-centrosymmetric $P\overline{1}0m2$ and those with x in the range of 7 to 10 are centrosymmetric. In addition, the space group of decagonal $Al_{65}Cu_{15}Co_{20}$ changes from $P\overline{1}0m2$ to $P10_5/mmc$ at about 600 °C [79].

3. HRTEM Analysis of QCs

When interacting with the atoms within a thin sample, the electron wave experiences phase shifts. These phase shifts contain the atomic arrangement information in the sample. With the suitable microscope parameters, the interference of the transmitted electron wave in the image plane generates the contrast of an HRTEM image. Therefore, the HRTEM image represents a projection of the lattice, which is folded with the phase contrast transfer properties of the microscope. Thus, for a correct image interpretation, various parameters such as defocus, specimen thickness and aberrations of the magnetic lenses need to be considered. Electrons interact very strongly with the atoms in the sample. Consequently, the phase changes of electron wave due to very small features like dislocations and interfaces can be recorded via HRTEM.

The local isomorphic nature of QCs makes it difficult to determine their structures solely by diffraction analysis, because different types of local arrangement can give rise to identical diffraction intensity distributions [80]. Thus, atomic-resolution HRTEM plays an indispensable role in the structural characterization, as they can represent the local atomic arrangement and cluster packing.

3.1. Icosahedral QCs

One year after the first QC was reported [1], the atomic arrangement in icosahedral Al–Mn was studied by Hiraga et al. [34] using HRTEM. Later, high-quality HRTEM images along the 5-fold axis of icosahedral Al–Mn–Si [81] and Al–Cu–Fe [33] etc. were also obtained. In the image taken along the 5-fold axis of Al–Cu–Fe (Figure 5, [33]), the bright dots are located homogeneously along the 5-fold directions with an angle of 36° without translational symmetry, as indicated by arrows in Figure 5a. Moreover, differently sized pentagons can be formed by connecting these spots (Figure 5b). This indicates that the atomic arrangement is ordered but aperiodic [82].

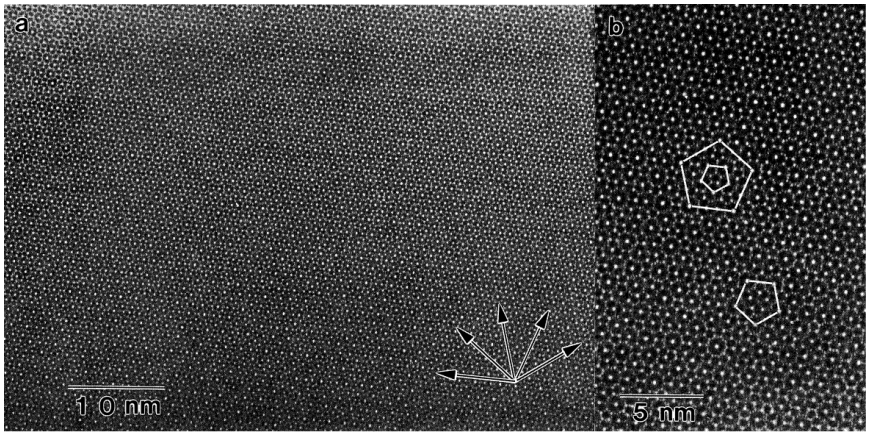

(**a**) (**b**)

Figure 5. HRTEM image taken along the 5-fold axis of icosahedral Al–Cu–Fe: (**a**) aperiodic but ordered distribution of bright dots; (**b**) enlargement of (**a**). The five arrows in (**a**) show that bright dots are lying along 5-fold symmetry directions; the pentagons in (**b**) indicate that bright dots can form pentagons of different sizes (reproduced from reference [33] with permission. Copyright 1988 The Japan Society of Applied Physics).

It should be noted that the quantitative interpretation of HR-TEM images of icosahedral phase depends strongly on specimen thickness, because dynamical diffraction effects can generate extra spots, leading to new diffraction patterns of reduced scale but similar symmetry [83].

3.2. Decagonal QCs

A decagonal columnar cluster is generally viewed as the building unit of decagonal QCs [84]. In the HRTEM images taken along their 10-fold axis, decagonal clusters appear as decagons, with the columnar cluster, tiling and defect information easily interpreted [28,84]. HRTEM observation of QCs helps one get a comprehensive understanding of their structures, providing an insight on their stabilization mechanism as to whether their quasiperiodic order is stabilized by energy or entropy.

Models can help one better understand the structures of QCs and different models have been proposed to describe quasiperiodic structures. Two-tile Penrose tiling was first proposed to cover the quasiperiodic plane [85]. In this tiling, two types of tiles—fat and skinny—match each other under a strict mathematical rule to form a perfect quasiperiodic pattern. After QCs were discovered, this tiling was employed to model quasiperiodic structures [86,87]. However, such a mathematical matching rule has no physical explanation on why the atoms should be arranged in this complicated way. Later, random packing of decagon clusters with 10-fold symmetry was proposed by Burkov [88]. In the random packing model, the overlapping of clusters is allowed, generating many types of configurations and a lot of chemical disorder. Some of the decagonal QCs discovered earlier support this model [62,89,90]. The random packing of this model means that entropy should be an important factor for the stability of these QCs.

Decagonal $Al_{72}Ni_{20}Co_8$ with high structural perfection tells a different story. Figure 6 [91] shows its HRTEM images taken along the periodic axis. From Figure 6a, it can be observed that the quasiperiodic structure can be well represented by the Gummelt tiling model [92], in which decagons are allowed to overlap with their neighbors according to the well-defined rule to form a quasiperiodic pattern. In contrast to the matching rule of Penrose tiling, the overlapping rule of Gummelt tiling has specific physical meaning [93]—Steinhardt and Jeong [94] have proven that the matching rule ensures that QCs have the maximum density. The unique overlapping of the clusters indicates that this decagonal phase is dominantly stabilized by energy. The atoms in the cluster center show mirror symmetry but not 10-fold symmetry (Figure 6b,c). Besides this type of decagonal cluster, another two types of decagonal clusters with mirror symmetry, 5-fold rotation symmetry and 10-fold symmetry

were proposed [95,96], as shown in Figure 7. First-principle total energy calculation [95,97] with Ni atoms used for all transition metal atoms shows that among the three types of symmetries the mirror-symmetry is the most favored energetically, followed by the 5-fold and 10-fold symmetry. That is, the highly-ordered atomic arrangement in this decagonal phase is energetically favored.

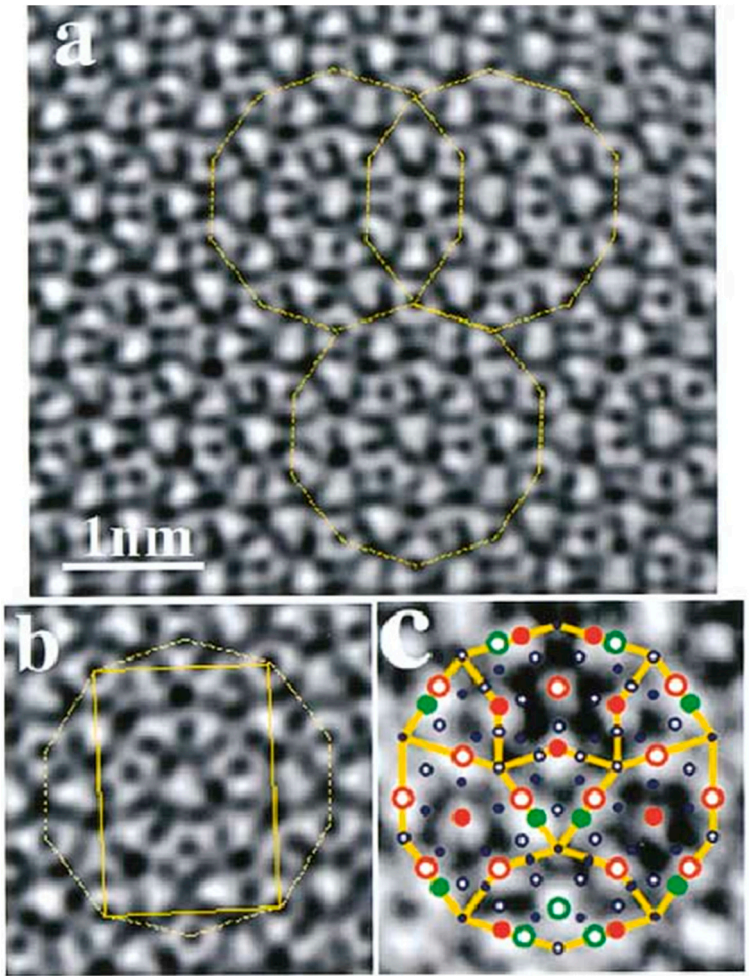

Figure 6. HRTEM images of decagonal $Al_{72}Ni_{20}Co_8$ with the background subtracted: (**a**) Gummelt tiling; (**b**) a representative decagonal cluster; and (**c**) the comparison between the mirror-symmetry model and the rectangular region in (**b**) (reproduced from reference [91] with permission).

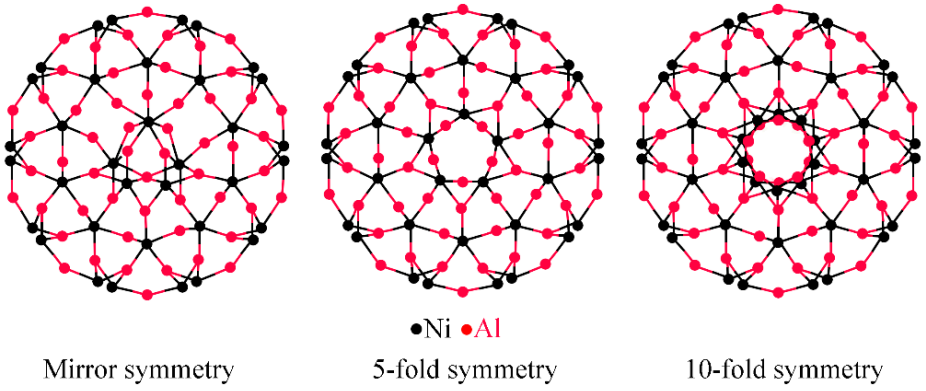

Figure 7. Models of decagonal clusters with three different symmetries (red dots indicate Al atoms, black dots transitional atoms. Reproduced from reference [95] with permission).

4. HAADF-STEM Analysis of QCs

In STEM mode, a very fine electron beam is used to scan the sample line by line. Due to the interaction between the electrons and the atoms within the sample, various kinds of signals are generated, including secondary electrons, backscattered electrons, transmitted electrons, elastically scattered electrons and inelastically scattered electrons. Subsequently, different detectors can be used to collect these signals to form images, which present the structural and/or compositional information of the sample. If a detector with a large inner radius is used to collect the incoherently scattered (not Bragg scattered) electrons at a very high angle, dark field images are obtained. The contrast of these dark field images is highly sensitive to variations in the atomic number of atoms in the sample. Therefore, this method is referred to as high-angle annular dark-field STEM (HAADF-STEM) or Z-contrast imaging, which can image local chemical composition on the nanometer scale.

The application of the STEM technique significantly facilitates the study of QCs, as the positions of heavy atoms can be directly observed. Owing to their periodicity along the 10-fold axis, the quasiperiodic atomic arrangement in decagonal QCs can be directly observed using high-resolution HAADF-STEM along this axis. Based on the atomic scale observation, structural details, such as the atomic arrangement within decagonal clusters, the tiling of these clusters and their chemical ordering, have been well investigated. It is worth noting that some structural information like chemical ordering can only be unveiled by high-resolution STEM.

Taniguchi et al. [46] succeeded in preparing highly perfect decagonal $Al_{64}Cu_{22}Co_{14}$ and studied it using electron diffraction and HAADF-STEM. The SAED and CBED patterns show that it is a non-centrosymmetric phase. The ultrahigh-resolution Z-contrast image taken along its periodic axis indicates that it is composed of decagonal atomic clusters with a diameter of 2 nm. The tiling of these atomic clusters can be obtained from the HAADF STEM image. Figure 8 shows the ultrahigh-resolution Z-contrast STEM image of decagonal $Al_{64}Cu_{22}Co_{14}$. In the image, the Al and Cu/Co (Cu and Co are neighbouring elements in the periodic table and not distinguishable in the Z-contrast STEM image) atomic columns are visualized with the Z-contrast. Obviously, the average of symmetry of decagonal clusters is 5-fold. However, it can be found that local chemical disorder occurs with Cu/Co substituting Al sites around the cluster center.

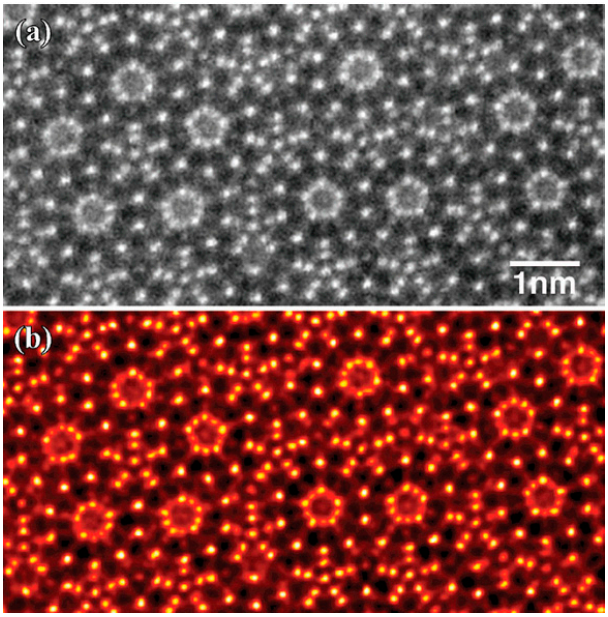

Figure 8. Ultrahigh-resolution HAADF-STEM images of decagonal $Al_{64}Cu_{22}Co_{14}$ taken along the periodic axis: (**a**) original image; and (**b**) image after maximum-entropy deconvolution (reproduced from reference [46] with permission).

The study of highly-ordered $Al_{58}Cu_{26}Ir_{16}$ decagonal phase by Seki et al. [98] through multivariate analysis of STEM images reveals that it is composed of two fundamental clusters with mirror or 10-fold symmetry and its atomic disorder is strongly restricted by these two symmetries.

Abe et al. [99] investigated the atomistic fluctuation in high-perfect decagonal $Al_{72}Ni_{20}Co_8$ using high-resolution HAADF STEM. The comparison of STEM images taken at 300 K with different angular ranges of the detector and at 1100 K verifies the occurrence of phasonic fluctuations. In addition, the HAADF STEM image further confirms that the atomic clusters of this decagonal phase possess a mirror-symmetry.

5. Outlook

The discussion in the previous sections suggests that great progress has been made in the study of quasicrystalline structures using TEM–basic structural details including symmetry, space group, defects and chemical disorder have been unveiled. However, due to their complexity, quasicrystalline structures are still not fully understood. For instance, the specific atomic arrangement within the 2D quasiperiodic layers of decagonal QCs and large clusters of icosahedral QCs has yet to be unambiguously determined.

It is difficult to obtain complete structural information about QCs merely by experimental techniques–diffraction and imaging. Diffraction analysis can only provide the globally averaged structural information, which may differ considerably from the local details [28,53]. The imaging by HRTEM and HAADF STEM can provide atomic-scale structural information. Such information, however, is averaged over the whole sample thickness (around 10 nm) [53]. This means that the atomic arrangement in each atomic layer cannot be directly determined by these imaging methods.

A combination of modelling and experiment would be essential to address the structures of QCs. Two main methods have been employed to geometrically describe quasicrystalline structures: high dimensional cut-and-project and space tiling [100]. The geometric models proposed can provide prescriptions for possible atomic configurations at both local and global levels, including the atomic arrangement of clusters and the puckering or tiling of these clusters [100–104]. If the models are verified or refined by experiments, they can be taken as the starting point for the theoretical calculation of QCs' physical properties [28,105]. Some work has been done by combining modelling and experiments to solve the structures of QCs. For example, Takakura et al. [106] proposed a structure model of binary icosahedral Yb–Cd QC and refined it with synchrotron X-ray diffraction data. However, more efforts are still needed as the structures of most QCs are not addressed thoroughly. Structural information by TEM will be vital for the verification and refinement of the models of QCs, given the fact that X-ray analysis can be misleading for complicated QCs [28].

The functional extension of TEM will also promote the study of QCs. The development of hot and cold stages will facilitate in-situ experiments. This is very important to correlate the structure and properties of QCs, especially after single-grain samples have been successfully prepared. The observation of structural changes caused by phase transformation, electron irradiation, chemical reaction, catalysis, hydrogen storage and indentation etc. will be realized [107]. It will be even possible to observe the real-time changes of atomic arrangement under various conditions.

Acknowledgments: This project was financially supported by the Nanyang Technological University Tier 1 Grant "Novel Metal Matrix Quasicrystal Composites with Strong Interface Chemical Bonding for Advanced Applications."

Author Contributions: Ruitao Li and Zhong Li drafted the manuscript and revised it. Zhili Dong and Khiam Aik Khor participated in the conception and discussion of the structure and contents. All the authors reviewed the manuscript.

Conflicts of Interest: The authors declare no conflict of interest.

Abbreviations

The following abbreviations are used in this manuscript:

QCs	Quasicrystals
TEM	Transmission electron microscopy
SAED	Selected area electron diffraction
CBED	Convergent beam electron diffraction
HRTEM	High-resolution transmission electron microscopy
STEM	Scanning transmission electron microscopy
HAADF	High angle annular dark field

References

1. Shechtman, D.; Blech, I.; Gratias, D.; Cahn, J.W. Metallic phase with long-range orientational order and no translational symmetry. *Phys. Rev. Lett.* **1984**, *53*, 1951–1953. [CrossRef]
2. Köster, U.; Liu, W.; Liebertz, H.; Michel, M. Mechanical properties of quasicrystalline and crystalline phases in Al–Cu–Fe alloys. *J. Non-Cryst. Solids* **1993**, *153*, 446–452. [CrossRef]
3. Zhou, C.; Cai, F.; Kong, J.; Gong, S.; Xu, H. A study on the tribological properties of low-pressure plasma-sprayed Al–Cu–Fe–Cr quasicrystalline coating on titanium alloy. *Surf. Coat. Technol.* **2004**, *187*, 225–229. [CrossRef]
4. Kang, S.; Dubois, J.; Von Stebut, J. Tribological properties of quasicrystalline coatings. *J. Mater. Res.* **1993**, *8*, 2471–2481. [CrossRef]
5. Pope, A.; Tritt, T.M.; Chernikov, M.; Feuerbacher, M. Thermal and electrical transport properties of the single-phase quasicrystalline material: $Al_{70.8}Pd_{20.9}Mn_{8.3}$. *Appl. Phys. Lett.* **1999**, *75*, 1854–1856. [CrossRef]
6. Gianno, K.; Sologubenko, A.; Chernikov, M.; Ott, H.; Fisher, I.; Canfield, P. Low-temperature thermal conductivity of a single-grain Y–Mg–Zn icosahedral quasicrystal. *Phys. Rev. B* **2000**, *62*, 292–300. [CrossRef]
7. Honda, Y.; Edagawa, K.; Yoshioka, A.; Hashimoto, T.; Takeuchi, S. Al–Pd–Re icosahedral quasicrystals and their low electrical conductivities. *Jpn. J. Appl. Phys.* **1994**, *33*, 4929–4935. [CrossRef]
8. Rivier, N. Non-stick quasicrystalline coatings. *J. Non-Cryst. Solids* **1993**, *153*, 458–462. [CrossRef]
9. Chernikov, M.; Paschen, S.; Felder, E.; Vorburger, P.; Ruzicka, B.; Degiorgi, L.; Ott, H.; Fisher, I.; Canfield, P. Low-temperature transport, thermal, and optical properties of single-grain quasicrystals of icosahedral phases in the Y–Mg–Zn and Tb–Mg–Zn alloy systems. *Phys. Rev. B* **2000**, *62*, 262–272. [CrossRef]
10. Demange, V.; Milandri, A.; De Weerd, M.; Machizaud, F.; Jeandel, G.; Dubois, J. Optical conductivity of Al–Cr–Fe approximant compounds. *Phys. Rev. B* **2002**, *65*, 144205. [CrossRef]
11. Dubois, J.-M. Properties-and applications of quasicrystals and complex metallic alloys. *Chem. Soc. Rev.* **2012**, *41*, 6760–6777. [CrossRef] [PubMed]
12. Dubois, J.-M. New prospects from potential applications of quasicrystalline materials. *Mater. Sci. Eng. A* **2000**, *294*, 4–9. [CrossRef]
13. Fleury, E.; Lee, S.; Kim, W.; Kim, D. Effects of air plasma spraying parameters on the Al–Cu–Fe quasicrystalline coating layer. *J. Non-Cryst. Solids* **2000**, *278*, 194–204. [CrossRef]
14. Cai, F.; Zhou, C.; Wang, N.; Gong, S.; Xu, H. Wear behavior of low-pressure plasma-sprayed AlCuFe quasicrystalline coating on titanium alloy. *Vacuum* **2006**, *81*, 85–90. [CrossRef]
15. Silva Guedes de Lima, B.A.; Medeiros Gomes, R.; Guedes de Lima, S.J.; Dragoe, D.; Barthes-Labrousse, M.-G.; Kouitat-Njiwa, R.; Dubois, J.-M. Self-lubricating, low-friction, wear-resistant al-based quasicrystalline coatings. *Sci. Technol. Adv. Mater.* **2016**, *17*, 71–79. [CrossRef]
16. Tian, Y.; Huang, H.; Yuan, G.; Ding, W. Microstructure evolution and mechanical properties of quasicrystal-reinforced Mg–Zn–Gd alloy processed by cyclic extrusion and compression. *J. Alloy. Compd.* **2015**, *626*, 42–48. [CrossRef]
17. Li, R.; Dong, Z.; Khor, K. Al–Cr–Fe quasicrystals as novel reinforcements in Ti based composites consolidated using high pressure spark plasma sintering. *Mater. Des.* **2016**, *102*, 255–263. [CrossRef]
18. Williams, D.B.; Carter, C.B. The transmission electron microscope. In *Transmission Electron Microscopy*; Springer: New York, NY, USA, 1996; pp. 3–17.
19. Srivastava, V.; Huttunen-Saarivirta, E.; Cui, C.; Uhlenwinkel, V.; Schulz, A.; Mukhopadhyay, N. Bulk synthesis by spray forming of Al–Cu–Fe and Al–Cu–Fe–Sn alloys containing a quasicrystalline phase. *J. Alloy. Compd.* **2014**, *597*, 258–268. [CrossRef]

20. Alhamidi, A.; Horita, Z. Grain refinement and high strain rate superplasticity in alumunium 2024 alloy processed by high-pressure torsion. *Mater. Sci. Eng. A* **2015**, *622*, 139–145. [CrossRef]
21. Oh, K.; Ahn, S.; Eom, K.; Jung, K.; Kwon, H. Observation of passive films on Fe$-_{20}$Cr$-_{x}$Ni (x=0, 10, 20wt%) alloys using TEM and Cs-corrected STEM–EELS. *Corros. Sci.* **2014**, *79*, 34–40. [CrossRef]
22. Chen, J.; Zandbergen, H.; Van Dyck, D. Atomic imaging in aberration-corrected high-resolution transmission electron microscopy. *Ultramicroscopy* **2004**, *98*, 81–97. [CrossRef] [PubMed]
23. Wang, J.; Zeng, Z.; Weinberger, C.R.; Zhang, Z.; Zhu, T.; Mao, S.X. In situ atomic-scale observation of twinning-dominated deformation in nanoscale body-centred cubic tungsten. *Nat. Mater.* **2015**, *14*, 594–600. [CrossRef] [PubMed]
24. Kübel, C.; Voigt, A.; Schoenmakers, R.; Otten, M.; Su, D.; Lee, T.-C.; Carlsson, A.; Bradley, J. Recent advances in electron tomography: TEM and HAADF-STEM tomography for materials science and semiconductor applications. *Microsc. Microanal.* **2005**, *11*, 378–400. [CrossRef] [PubMed]
25. Muller, D.A. Structure and bonding at the atomic scale by scanning transmission electron microscopy. *Nat. Mater.* **2009**, *8*, 263–270. [CrossRef] [PubMed]
26. Yang, J.C.; Small, M.W.; Grieshaber, R.V.; Nuzzo, R.G. Recent developments and applications of electron microscopy to heterogeneous catalysis. *Chem. Soc. Rev.* **2012**, *41*, 8179–8194. [CrossRef] [PubMed]
27. Jacobson, K.; Mouritsen, O.G.; Anderson, R.G. Lipid rafts: At a crossroad between cell biology and physics. *Nat. Cell Biol.* **2007**, *9*, 7–14. [CrossRef] [PubMed]
28. Abe, E. Electron microscopy of quasicrystals—Where are the atoms? *Chem. Soc. Rev.* **2012**, *41*, 6787–6798. [CrossRef] [PubMed]
29. Liu, J.; Yang, Z.; Ye, H. In situ transmission electron microscopy investigation of quasicrystal-crystal transformations in Mg–Zn–Y alloys. *J. Alloy. Compd.* **2015**, *621*, 179–188. [CrossRef]
30. Widjaja, E.; Marks, L. Microstructural evolution in Al–Cu–Fe quasicrystalline thin films. *Thin Solid Films* **2003**, *441*, 63–71. [CrossRef]
31. Tsuda, K. Convergent-beam electron diffraction and electron microscopy study of decagonal quasicrystals of Al–Ni–Rh and Al–Ni–Ir. *Philos. Mag. Lett.* **1996**, *73*, 271–278. [CrossRef]
32. Li, R.; Dong, Z.; Murugan, V.K.; Zhang, Z.; Khor, K. Microstructure characterization of Al–Cr–Fe quasicrystals sintered using spark plasma sintering. *Mater. Charact.* **2015**, *110*, 264–271. [CrossRef]
33. Hiraga, K.; Zhang, B.-P.; Hirabayashi, M.; Inoue, A.; Masumoto, T. Highly ordered icosahedral quasicrystal of Al–Cu–Fe alloy studied by electron diffraction and high-resolution electron microscopy. *Jpn. J. Appl. Phys.* **1988**, *27*, L951–L953. [CrossRef]
34. Hiraga, K.; Hirabayashi, M.; Inoue, A.; Masumoto, T. Icosahedral quasicrystals of a melt-quenched Al-Mn alloy observed by high-resolution electron microscopy. *Sci. Rep. Res. Inst. Tohoku Univ. Ser. A* **1985**, *32*, 309–314.
35. Hiraga, K.; Yasuhara, A.; Yamamoto, K.; Yubuta, K. The structure of an Al–Rh–Cu decagonal quasicrystal studied by spherical aberration (Cs)-corrected scanning transmission electron microscopy. *Philos. Mag.* **2015**, *95*, 1524–1535. [CrossRef]
36. Yasuhara, A.; Saito, K.; Hiraga, K. Direct observations of aperiodic arrangements of transition-metal atoms in Al–Co–Ni decagonal quasicrystals by cs-corrected haadf-stem. In *Aperiodic Crystals*; Springer: Dordrecht, The Netherlands, 2013; pp. 219–224.
37. Rokhsar, D.S.; Mermin, N.D.; Wright, D.C. Rudimentary quasicrystallography: The icosahedral and decagonal reciprocal lattices. *Phys. Rev. B* **1987**, *35*, 5487–5495. [CrossRef]
38. Ebalard, S.; Spaepen, F. The body-centered-cubic-type icosahedral reciprocal lattice of the Al–Cu–Fe quasi-periodic crystal. *J. Mater. Res.* **1989**, *4*, 39–43. [CrossRef]
39. Ohhashi, S.; Hasegawa, J.; Takeuchi, S.; Tsai, A. Crystal growth of quasicrystal and partial phase diagram involving quasicrystal in the Ag–In–Yb system. *Philos. Mag.* **2007**, *87*, 3089–3094. [CrossRef]
40. Guo, J.; Abe, E.; Tsai, A.-P. Stable icosahedral quasicrystals in the Cd–Mg–RE (RE = rare earth element) systems. *Jpn. J. Appl. Phys.* **2000**, *39*, L770–L771. [CrossRef]
41. Tsai, A.-P.; Inoue, A.; Masumoto, T. A stable quasicrystal in Al–Cu–Fe system. *Jpn. J. Appl. Phys.* **1987**, *26*, L1505–L1507. [CrossRef]
42. Tsai, A.; Inoue, A.; Yokoyama, Y.; Masumoto, T. Stable icosahedral Al–Pd–Mn and Al–Pd–Re alloys. *Mater. Trans. JIM* **1990**, *31*, 98–103. [CrossRef]

43. Niikura, B.A.; Tsai, A.; Inoue, A.; Masumoto, T. Stable Zn-Mg-rare-earth face-centred icosahedral alloys with pentagonal dodecahedral solidification morphology. *Philos. Mag. Lett.* **1994**, *69*, 351–355. [CrossRef]
44. Kuczera, P.; Wolny, J.; Steurer, W. Comparative structural study of decagonal quasicrystals in the systems Al–Cu–Me (Me = Co, Rh, Ir). *Acta Crystallogr. Sect. B Struct. Sci.* **2012**, *68*, 578–589. [CrossRef] [PubMed]
45. Hiraga, K. Structural study of a superlattice Al–Ni–Ru decagonal quasicrystal using high-resolution electron microscopy and a high-angle annular dark-field technique. *Philos. Mag. Lett.* **2001**, *81*, 187–195. [CrossRef]
46. Taniguchi, S.; Abe, E. Highly-perfect decagonal quasicrystalline $Al_{64}Cu_{22}Co_{14}$ with non-centrosymmetry. *Philos. Mag.* **2008**, *88*, 1949–1958. [CrossRef]
47. Yan, Y.; Wang, R. The burgers vector of an edge dislocation in an $Al_{70}Co_{15}Ni_{15}$ decagonal quasicrystal determined by means of convergent-beam electron diffraction. *J. Phys. Condens. Matter* **1993**, *5*, L195–L200. [CrossRef]
48. He, L.X.; Wu, Y.; Kuo, K. Decagonal quasicrystals with different periodicities along the tenfold axis in rapidly solidified $Al_{65}Cu_{20}M_{15}$ (M = Mn, Fe, Co or Ni). *J. Mater. Sci. Lett.* **1988**, *7*, 1284–1286. [CrossRef]
49. Pavlyuchkov, D.; Balanetskyy, S.; Kowalski, W.; Surowiec, M.; Grushko, B. Stable decagonal quasicrystals in the Al–Fe–Cr and Al–Fe–Mn alloy systems. *J. Alloy. Compd.* **2009**, *477*, L41–L44. [CrossRef]
50. Sun, W.; Hiraga, K. A new highly ordered Al–Ni–Ru decagonal quasicrystal with 1.6 nm periodicity. *Philos. Mag. Lett.* **2000**, *80*, 157–164. [CrossRef]
51. Tsai, A.; Inoue, A.; Masumoto, T. Stable decagonal quasicrystals with a periodicity of 1.6 nm in Al–Pd–(Fe, Ru or Os) alloys. *Philos. Mag. Lett.* **1991**, *64*, 163–167. [CrossRef]
52. Ranganathan, S.; Chattopadhyay, K.; Singh, A.; Kelton, K. Decagonal quasicrystals. *Prog. Mater. Sci.* **1997**, *41*, 195–240. [CrossRef]
53. Steurer, W.; Deloudi, S. Decagonal quasicrystals—what has been achieved? *C. R. Phys.* **2014**, *15*, 40–47. [CrossRef]
54. Ritsch, S. Highly perfect decagonal Al–Co–Ni quasicrystals. *Philos. Mag. Lett.* **1996**, *74*, 99–106. [CrossRef]
55. Li, X. Structure ofthe Al-Rh-Cu decagonal quasicrystal studied by high-resolution electron microscopy. *Philos. Mag. Lett.* **1996**, *74*, 247–252. [CrossRef]
56. Abe, E.; Tsai, A. Structure of a metastable Al_3Ni decagonal quasicrystal: Comparison with a highly perfect $Al_{72}Ni_{20}Co_8$. *J. Alloy. Compd.* **2002**, *342*, 96–100. [CrossRef]
57. Beeli, C. High-resolution electron microscopy of quasicrystals. *Mater. Sci. Eng. A* **2000**, *294*, 23–28. [CrossRef]
58. Edagawa, K.; Ichihara, M.; Suzuki, K.; Takeuchi, S. New type of decagonal quasicrystal with superlattice order in Al–Ni–Co alloy. *Philos. Mag. Lett.* **1992**, *66*, 19–25. [CrossRef]
59. Saito, K.; Ohsuna, T.; Sun, W.; Hiraga, K. Reversible phase changes of Ni-rich Al–Co–Ni decagonal quasicrystals studied by means of transmission electron microscopy and thermal analysis. *J. Alloy. Compd.* **2004**, *372*, 169–175. [CrossRef]
60. Pramanick, A.; Mandal, R.; Sastry, G. Effect of composition on the streaking and diffuse intensity in decagonal phase in $Al_{70-X}Co_{15}Cu_{X+Y}Ni_{15-Y}$ system. *Mater. Sci. Eng. A* **2000**, *294*, 173–177. [CrossRef]
61. Saito, M.; Tanaka, M.; Tsai, A.P.; Inoue, A.; Masumoto, T. Space group determination of decagonal quasicrystals of an $Al_{70}Ni_{15}Fe_{15}$ alloy using convergent-beam electron diffraction. *Jpn. J. Appl. Phys.* **1992**, *31*, L109–L112. [CrossRef]
62. Hiraga, K.; Lincoln, F.J.; Sun, W. Structure and structural change of Al–Ni–Co decagonal quasicrystal by high-resolution electron microscopy. *Mater. Trans. JIM* **1991**, *32*, 308–314. [CrossRef]
63. Wang, N.; Chen, H.; Kuo, K. Two-dimensional quasicrystal with eightfold rotational symmetry. *Phys. Rev. Lett.* **1987**, *59*, 1010–1013. [CrossRef] [PubMed]
64. Cao, W.; Ye, H.; Kuo, K. A new octagonal quasicrystal and related crystalline phases in rapidly solidified Mn_4Si. *Phys. Status Solidi A* **1988**, *107*, 511–519. [CrossRef]
65. Wang, N.; Fung, K.K.; Kuo, K. Symmetry study of the Mn–Si–Al octagonal quasicrystal by convergent beam electron diffraction. *Appl. Phys. Lett.* **1988**, *52*, 2120–2121. [CrossRef]
66. Jiang, J.; Fung, K.; Kuo, K. Discommensurate microstructures in phason-strained octagonal quasicrystal phases of Mo–Cr–Ni. *Phys. Rev. Lett.* **1992**, *68*, 616–619. [CrossRef] [PubMed]
67. Chen, H.; Li, D.; Kuo, K. New type of two-dimensional quasicrystal with twelvefold rotational symmetry. *Phys. Rev. Lett.* **1988**, *60*, 1645–1648. [CrossRef] [PubMed]
68. Conrad, M.; Krumeich, F.; Harbrecht, B. A dodecagonal quasicrystalline chalcogenide. *Angew. Chem. Int. Ed.* **1998**, *37*, 1383–1386. [CrossRef]

69. Tanaka, M. Characterization of icosahedral quasicrystals by convergent-beam electron diffraction ((B) quasicrystals). *Sci. Rep. Res. Inst. Tohoku Univ. Ser. A* **1991**, *36*, 159–170.
70. Tanaka, M. Convergent-beam electron diffraction. *Acta Crystallogr. Sect. A Found. Crystallogr.* **1994**, *50*, 261–286. [CrossRef]
71. Tanaka, M.; Terauchi, M.; Kaneyama, T. *Convergent-Beam Electron Diffraction II*; Jeol: Tokyo, Japan, 1988; Volume 2.
72. Bendersky, L.; Kaufman, M. Determination of the point group of the icosahedral phase in an Al–Mn–Si alloy using convergent-beam electron diffraction. *Philos. Mag. B* **1986**, *53*, L75–L80. [CrossRef]
73. Cassada, W.; Shiflet, G.; Poon, S. Formation of an icosahedral phase by solid-state reaction. *Phys. Rev. Lett.* **1986**, *56*, 2276–2279. [CrossRef] [PubMed]
74. Hwang, J.; Doty, H.; Kaufman, M. Crystallographic studies on the iron-containing intermetallic phases in the 319-type aluminium casting alloys. *Philos. Mag.* **2008**, *88*, 607–619. [CrossRef]
75. Saitoh, K.; Tsuda, K.; Tanaka, M.; Tsai, A.; Inoue, A.; Masumoto, T. Convergent-beam electron diffraction and electron microscope study on decagonal quasicrystals of Al–Cu–Co and Al–Co alloys. *Mater. Sci. Eng. A* **1994**, *181*, 805–810. [CrossRef]
76. Saitoh, K.; Tanaka, M.; Tsai, P. Structural study of an $Al_{73}Ni_{22}Fe_5$ decagonal quasicrystal by high-angle annular dark-field scanning transmission electron microscopy. *J. Electron Microsc.* **2001**, *50*, 197–203. [CrossRef]
77. Tsuda, K.; Nishida, Y.; Saitoh, K.; Tanaka, M.; Tsai, A.; Inoue, A.; Masumoto, T. Structure of Al–Ni–Co decagonal quasicrystals. *Philos. Mag. A* **1996**, *74*, 697–708. [CrossRef]
78. Tanaka, M.; Tsuda, K.; Terauchi, M.; Fujiwara, A.; Tsai, A.; Inoue, A.; Masumoto, T. Electron diffraction and electron microscope study on decagonal quasicrystals on Al–Ni–Fe alloys. *J. Non-Cryst. Solids* **1993**, *153*, 98–102. [CrossRef]
79. Saitoh, K.; Tsuda, K.; Tanaka, M.; Tsai, A.; Inoue, A.; Masumoto, T. Electron microscope study of the symmetry of the basic atom cluster and a structural change of decagonal quasicrystals of Al–Cu–Co alloys. *Philos. Mag. A* **1996**, *73*, 387–398. [CrossRef]
80. Stadnik, Z.M. *Physical Properties of Quasicrystals*; Springer Science & Business Media: Berlin, Germany, 2012; Volume 126.
81. Hiraga, K.; Hirabayashi, M.; Inoue, A.; Masumoto, T. High-resolution electron microscopy of Al–Mn–Si icosahedral and Al–Mn decagonal quasicrystals. *J. Microsc.* **1987**, *146*, 245–260. [CrossRef]
82. Tsai, A.-P. Discovery of stable icosahedral quasicrystals: Progress in understanding structure and properties. *Chem. Soc. Rev.* **2013**, *42*, 5352–5365. [CrossRef] [PubMed]
83. Zupanič, F.; Bončina, T.; Križman, A.; Grogger, W.; Gspan, C.; Markoli, B.; Spaić, S. Quasicrystalline phase in melt-spun Al–Mn–Be ribbons. *J. Alloy. Compd.* **2008**, *452*, 343–347. [CrossRef]
84. Abe, E.; Yan, Y.; Pennycook, S.J. Quasicrystals as cluster aggregates. *Nat. Mater.* **2004**, *3*, 759–767. [CrossRef] [PubMed]
85. Penrose, R. The role of aesthetics in pure and applied mathematical research. *Bull. Inst. Math. Appl.* **1974**, *10*, 266–271.
86. Bursill, L.; Lin, P.J. Penrose tiling observed in a quasi-crystal. *Nature* **1985**, *316*, 50–51. [CrossRef]
87. Levine, D.; Steinhardt, P.J. Quasicrystals: A new class of ordered structures. *Phys. Rev. Lett.* **1984**, *53*, 2477–2480. [CrossRef]
88. Burkov, S. Structure model of the Al–Cu–Co decagonal quasicrystal. *Phys. Rev. Lett.* **1991**, *67*, 614–617. [CrossRef] [PubMed]
89. Chen, H.; Burkov, S.; He, Y.; Poon, S.; Shiflet, G. High-resolution electron-microscopy study and structure modeling of the stable decagonal Al-Cu-Co quasicrystal. *Phys. Rev. Lett.* **1990**, *65*, 72–75. [CrossRef] [PubMed]
90. Mukhopadhyay, N.; Sastry, G.; Weatherly, G. Electron microscopy analysis of decagonal quasicrystals in the Al–Cu–Co–Si system. *Philos. Mag. A* **2000**, *80*, 1795–1809. [CrossRef]
91. Abe, E.; Saitoh, K.; Takakura, H.; Tsai, A.; Steinhardt, P.; Jeong, H.-C. Quasi-unit-cell model for an Al–Ni–Co ideal quasicrystal based on clusters with broken tenfold symmetry. *Phys. Rev. Lett.* **2000**, *84*, 4609–4612. [CrossRef] [PubMed]
92. Gummelt, P. Construction of penrose tilings by a single aperiodic protoset. In Proceedings of the 5th International Conference on Quasicrystals, Avignon, France, 22–26 May 1995; pp. 84–87.

93. Steinhardt, P.J.; Jeong, H.-C.; Saitoh, K.; Tanaka, M.; Abe, E.; Tsai, A. Experimental verification of the quasi-unit-cell model of quasicrystal structure. *Nature* **1998**, *396*, 55–57. [CrossRef]
94. Steinhardt, P.J.; Jeong, H.-C. A simpler approach to penrose tiling with implications for quasicrystal formation. *Nature* **1996**, *382*, 431–432. [CrossRef]
95. Yan, Y.; Pennycook, S.J. Chemical ordering in $Al_{72}Ni_{20}Co_8$ decagonal quasicrystals. *Phys. Rev. Lett.* **2001**, *86*, 1542–1545. [CrossRef] [PubMed]
96. Yan, Y.; Pennycook, S.J. Alloys: Atomic structure of the quasicrystal $Al_{72}Ni_{20}Co_8$. *Nature* **2000**, *403*, 266–267. [CrossRef] [PubMed]
97. Mihalkovič, M.; Al-Lehyani, I.; Cockayne, E.; Henley, C.; Moghadam, N.; Moriarty, J.; Wang, Y.; Widom, M. Total-energy-based prediction of a quasicrystal structure. *Phys. Rev. B* **2002**, *65*, 104205. [CrossRef]
98. Seki, T.; Abe, E. Local cluster symmetry of a highly ordered quasicrystalline $Al_{58}Cu_{26}Ir_{16}$ extracted through multivariate analysis of STEM images. *Microscopy* **2015**, *64*, 341–349. [CrossRef] [PubMed]
99. Abe, E.; Pennycook, S.; Tsai, A. Direct observation of a local thermal vibration anomaly in a quasicrystal. *Nature* **2003**, *421*, 347–350. [CrossRef] [PubMed]
100. De Boissieu, M. Atomic structure of quasicrystals. *Struct. Chem.* **2012**, *23*, 965–976. [CrossRef]
101. Yamamoto, A.; Takakura, H.; Tsai, A.P. Six-dimensional model of icosahedral Al–Pd–Mn quasicrystals. *Phys. Rev. B* **2003**, *68*. [CrossRef]
102. Yamamoto, A.; Takakura, H.; Abe, E. Five-dimensional model of the S1-superstructure phase in Al−Ni−Co quasicrystals. *Phys. Rev. B* **2005**, *72*. [CrossRef]
103. Yamamoto, A.; Weber, S. Five-dimensional superstructure model of decagonal Al–Ni–Co quasicrystals. *Phys. Rev. Lett.* **1997**, *78*, 4430–4433. [CrossRef]
104. Mihalkovič, M.; Zhu, W.-J.; Henley, C.; Oxborrow, M. Icosahedral quasicrystal decoration models. I. Geometrical principles. *Phys. Rev. B* **1996**, *53*, 9002–9020. [CrossRef]
105. Fujita, N.; Takano, H.; Yamamoto, A.; Tsai, A.-P. Cluster-packing geometry for Al-based f-type icosahedral alloys. *Acta Crystallogr. Sect. A Found. Crystallogr.* **2013**, *69*, 322–340. [CrossRef]
106. Takakura, H.; Gómez, C.P.; Yamamoto, A.; De Boissieu, M.; Tsai, A.P. Atomic structure of the binary icosahedral Yb–Cd quasicrystal. *Nat. Mater.* **2007**, *6*, 58–63. [CrossRef] [PubMed]
107. Zheng, H.; Meng, Y.S.; Zhu, Y. Frontiers of in situ electron microscopy. *MRS Bull.* **2015**, *40*, 12–18. [CrossRef]